Supplementary Material

Crystallography on a chip

Arash Zarrine-Afsar[1], Thomas R.M. Barends[2,3*], Christina Müller[1*], Martin R. Fuchs[4], Lukas Lomb[2,3], Ilme Schlichting[2,3] and R.J. Dwayne Miller[1]

[1] Max Planck Research Group for Structural Dynamics, Center for Free-Electron Laser Science, Department of Physics, University of Hamburg, Notkestrasse 85, 22607 Hamburg, Germany and Department of Chemistry and Physics, University of Toronto, 80 St George Street, Toronto, ON, M5S-3H6, Canada
[2] Max Planck Institute for Medical Research, Jahnstrasse 29, 69120 Heidelberg, Germany
[3]Max Planck Advanced Study Group, Center for Free-Electron Laser Science, Notkestrasse 85, 22607 Hamburg, Germany
[4] Swiss Light Source, Paul Scherrer Institute, CH-5232 Villigen, PSI, Switzerland
* These authors contributed equally to this work.
Email: dwayne.miller@mpsd.cfel.de (chip) or ilme.schlichting@mpimf-heidelberg.mpg.de (x-ray diffraction analysis)

Table of Contents

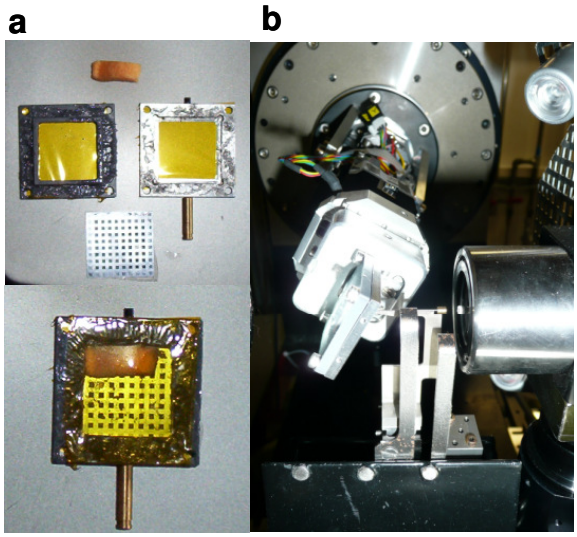

Supplementary Fig. 1 The chip holder structure and mounting of the chip. (a) Components of the chip holder: the chip, the reservoir sponge, frames with polyimide film, and a brass pin for mounting on a standard magnetic base (upper panel), as well as the completed assembly (lower panel). (b) The chip holder mounted on the goniometer of beam line X10SA at the Swiss Light Source (SLS). The holder is tilted on the rotation axis, with a Mo tube collimator visible on the right hand side in close proximity to the holder.

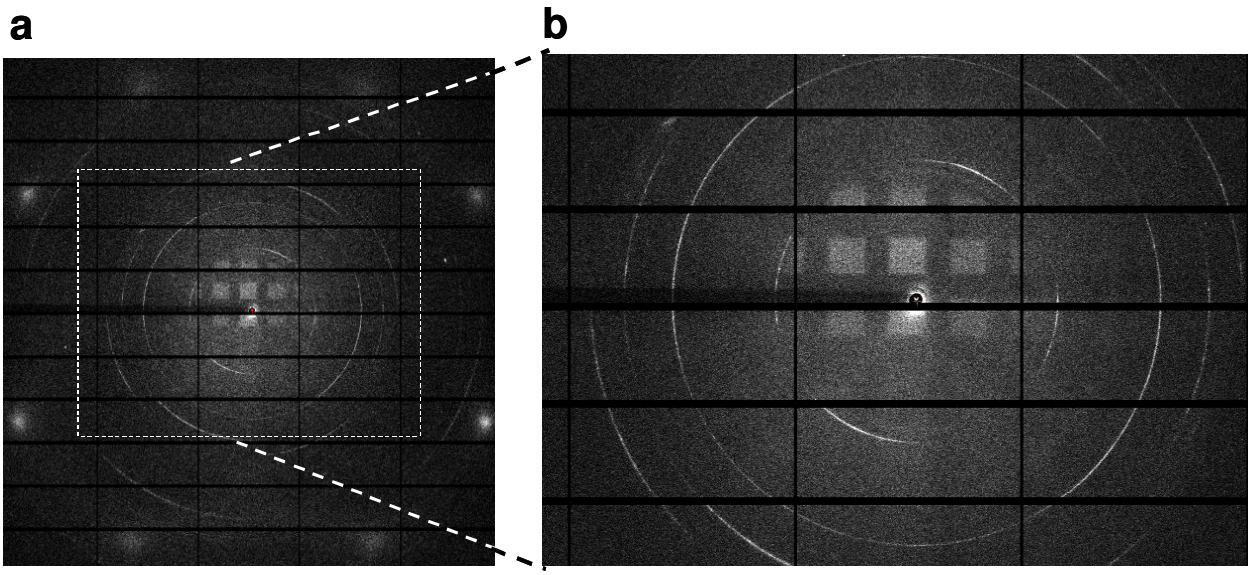

Supplementary Fig. 2 Shadow from an unloaded empty chip grid (silicon mesh and kapton film) in the absence of a collimating tube in close proximity, illustrating the effect of upstream air scatter. Spots from crystalline silicon, rings from polyimide as well as a 'checkerboard' pattern resulting from upstream air scatter are visible.

Supplementary Methods

Microfabrication of the chip

The chip as shown in **Fig.1** was created by the adhesion of a 10 μm thick polyimide tape with silicone adhesive on one side (Matrix Technology, Markham, ON, Canada) to a silicon mesh. Amorphous glass beads with size distributions of <106 μm, as well as 4-8 μm in diameter (Sigma Aldrich, Oakville, ON, Canada and Cospheric, Santa Barbara, CA, USA), were deposited into the wells, and attached to the polyimide by the adhesive on the film. Excess beads were blown off gently by a blast of compressed air.

To produce the silicon mesh, we used standard silicon technology and photolithography. Details of the technical steps and instrumentation are as described previously (Zarrine-Afsar *et al.*, 2011). The well structures that form the grid are arranged in block compartments spaced ~1mm apart to secure stability of the mesh structure. Within each compartment the wells were adjusted in size to accommodate the crystals in the array to be assembled, ~60 μm (**Fig. 1a**) and ~45 μm (**Fig. 1b**). To adjust the thickness of the grid the area on the backside of the wafer that corresponds to each grid compartment was etched using standard methods. Here, the thickness of the silicon mesh was 30-40 μm to accommodate the sizes of ferritin and lysozyme crystals used.

Chip holder design to keep mounted crystals hydrated

In order to keep the crystals hydrated during room-temperature data collection, we designed a chip holder that uses an absorbent sponge soaked in mother liquor, providing a reservoir to ensure the correct liquid vapor pressure in between two polypropylene (or polyimide) films **(Supplementary Fig. 1**).

Model systems tested

Brick-shaped lysozyme crystals were used to evaluate the performance of the chip in sampling of the reciprocal space for low-aspect ratio plate-or brick-shaped crystals that are expected to lie flat on the surface of the chip. A uniformly shaped, brick-like population of lysozyme crystals was obtained by batch crystallization. 60 μl of hen egg white lysozyme (60 mg/ml in 0.1 M Na acetate pH 3.4) were mixed with 140 μl of precipitant solution (7-10 % (w/v) NaCl in 0.1 M Na acetate pH 4.5) in the wells of Linbro plates to obtain brick-shaped crystals of ~5-10, and ~30-50 micron lengths, respectively. Horse spleen ferritin crystals were grown in the hanging drop geometry by mixing (2 μl of protein (30 mg/ml) and precipitant solution, respectively. The drops were equilibrated against 1 ml of precipitant solution (3-5 mM $CdSO_4$, 100-200 mM ammonium sulfate). Diamond shaped crystals of 30 and 60 μm diameter were mounted in the chips. Diffraction data were collected at the Swiss Light Source as described below. The statistics are given in **Table 1.**

Loading the chip (dynamic wetting)

To load the chip a small (1-2μl) amount of crystal suspension was laterally moved across the chip surface to self-localize crystals on the hydrophilic patches provided by the beads. The silicon mesh guided the localization of beads to prescribed locations on the surface of the polyimide film, and also aided in inducing instability in the equilibrium liquid 'contact line' between the drop and the surface (Zarrine-Afsar *et al.*, 2011) upon moving the liquid on the top surface. To prevent multiple hits (i.e. multiple crystals localizing to the same well) a suitable

dilution of crystal suspension must be used. Here, the chip concept also offers size exclusion sorting capabilities as described in our previous work (Zarrine-Afsar *et al.*, 2011). It must be noted that the beads, or irregularly shaped particles, may be further modified to contain a suite of affinity ligands to further facilitate the crystal capture (provided the target site is accessible in the crystal), or use non-specific forces such as electrostatic interactions to meet this need. This becomes important when the buoyancy of the crystal in the mother liquor is such that the crystals float in the mother liquor, not making significant contacts with the beads to adopt orientations consistent with what is dictated by the roughness on the surface.

Diffraction data collection and their analysis

Diffraction data were collected at the Swiss Light Source using a Pilatus 6M hybrid pixel detector and 1° rotations, with the crystals kept at 24 °C. Close to 150 lysozyme crystals were exposed to X-rays to determine the relative orientation of the crystal lattice to the X-ray beam and detector laboratory frame by indexing with XDS (Kabsch, 1988) (see **Figure 2**). 30° of data were collected of a single ferritin crystal to test the influence of the chip and the holder assembly on the data quality achievable with the chip design (e.g. background scattering). Data were processed using the program XDS (Kabsch, 1988) (see **Table 1** for details).

Structure refinement was carried out against deposited lysozyme (PDB:2YVB) and ferritin (PDB:2V2S) structures using Refmac5 (Murshudov *et al.*, 1997) and Phenix (Adams *et al.*, 2010) suite of programs, and the quality of the models was visually verified with COOT (Emsley & Cowtan, 2004) and CCP4 (Bailey, 1994).

Crystal orientations were determined by calculating the mis-setting angles between the crystal lattice and the laboratory frame from the XDS orientation matrix XPARM (Kabsch, 1988). If a tetragonal lysozyme crystal is aligned with *a* along x, *b* along y and *c* along z then the orientation matrix *X* from XDS defining the laboratory coordinates of the unit cell axes for an unrotated crystal will be

$$X_0 = \begin{bmatrix} a & 0 & 0 \\ 0 & b & 0 \\ 0 & 0 & c \end{bmatrix}$$

as the cell angles are 90˚ in this case. In a rotated crystal, on the other hand, a rotation matrix *O* has operated on the above matrix X_0 to yield the matrix X as the output in file XPARM.XDS from program XDS:

$$X = OX_0 = O\begin{bmatrix} a & 0 & 0 \\ 0 & b & 0 \\ 0 & 0 & c \end{bmatrix}$$

O can be defined as the product of three matrices, each representing a rotation around a different axis:

$$\Phi = \begin{bmatrix} \cos\varphi & -\sin\varphi & 0 \\ \sin\varphi & \cos\varphi & 0 \\ 0 & 0 & 1 \end{bmatrix}, \Psi = \begin{bmatrix} \cos\psi & 0 & -\sin\psi \\ 0 & 1 & 0 \\ \sin\psi & 0 & \cos\psi \end{bmatrix}, \Omega = \begin{bmatrix} 1 & 0 & 0 \\ 0 & \cos\omega & -\sin\omega \\ 0 & \sin\omega & \cos\omega \end{bmatrix}$$

$$O = \Phi\Psi\Omega = \begin{bmatrix} \cos\varphi\cos\psi & -\sin\omega\cos\varphi\sin\psi - \cos\omega\sin\varphi & \sin\omega\sin\varphi - \cos\omega\cos\varphi\sin\psi \\ \sin\varphi\cos\psi & \cos\omega\cos\varphi - \sin\omega\sin\varphi\sin\psi & -\cos\omega\sin\varphi\sin\psi - \sin\omega\cos\varphi \\ \sin\psi & \sin\omega\cos\psi & \cos\omega\cos\psi \end{bmatrix}$$

Where Φ, Ψ, and Ω represent rotations around the XDS z, y and x axes, respectively. Inversion of the matrix X_0 and multiplication with the rotated matrix X yields matrix O:

$$OX_0 = X$$
$$OX_0X_0^{-1} = XX_0^{-1}$$
$$O = XX_0^{-1}$$

The angles φ, ψ, and ω can now be read from its elements.

References

Adams, P. D., Afonine, P. V., Bunkoczi, G., Chen, V. B., Davis, I. W., Echols, N., Headd, J. J., Hung, L. W., Kapral, G. J., Grosse-Kunstleve, R. W., McCoy, A. J., Moriarty, N. W., Oeffner, R., Read, R. J., Richardson, D. C., Richardson, J. S., Terwilliger, T. C. & Zwart, P. H. (2010). *Acta Crystallogr D* **66**, 213-221.

Bailey, S. (1994). *Acta Crystallogr D* **50**, 760-763.

Emsley, P. & Cowtan, K. (2004). *Acta Crystallogr D* **60**, 2126-2132.

Kabsch, W. (1988). *Journal of Appl. Cryst.* **21**, 916-924.

Murshudov, G. N., Vagin, A. A. & Dodson, E. J. (1997). *Acta Crystallogr D* **53**, 240-255.

Zarrine-Afsar, A., Muller, C., Talbot, F. O. & Miller, R. J. D. (2011). *Anal Chem* **83**, 767-773.